Stem Cell Research (2014) 12, 400–414

Available online at www.sciencedirect.com

ScienceDirect

www.elsevier.com/locate/scr

Topoisomerase I inhibitor, camptothecin, induces apoptogenic signaling in human embryonic stem cells

Carolina Paola García [1], Guillermo Agustín Videla Richardson [1], Leonardo Romorini, Santiago Gabriel Miriuka, Gustavo Emilio Sevlever, María Elida Scassa*

Laboratorio de Investigación aplicada a Neurociencias-LIAN-Fundación para la Lucha contra las Enfermedades Neurológicas de la Infancia-FLENI, Ruta 9, Km 52.5, B1625XAF Escobar, Provincia de Buenos Aires, Argentina

Received 1 August 2013; received in revised form 27 November 2013; accepted 4 December 2013
Available online 14 December 2013

Abstract Embryonic stem cells (ESCs) need to maintain their genomic integrity in response to DNA damage to safeguard the integrity of the organism. DNA double strand breaks (DSBs) are one of the most lethal forms of DNA damage and, if not repaired correctly, they can lead to cell death, genomic instability and cancer. How human ESCs (hESCs) maintain genomic integrity in response to agents that cause DSBs is relatively unclear. In the present study we aim to determine the hESC response to the DSB inducing agent camptothecin (CPT). We find that hESCs are hypersensitive to CPT, as evidenced by high levels of apoptosis. CPT treatment leads to DNA-damage sensor kinase (ATM and DNA-PKcs) phosphorylation on serine 1981 and serine 2056, respectively. Activation of ATM and DNA-PKcs was followed by histone H2AX phosphorylation on Ser 139, a sensitive reporter of DNA damage. Nuclear accumulation and ATM-dependent phosphorylation of p53 on serine 15 were also observed. Remarkably, hESC viability was further decreased when ATM or DNA-PKcs kinase activity was impaired by the use of specific inhibitors. The hypersensitivity to CPT treatment was markedly reduced by blocking p53 translocation to mitochondria with pifithrin-μ. Importantly, programmed cell death was achieved in the absence of the cyclin dependent kinase inhibitor, $p21^{Waf1}$, a bona fide p53 target gene. Conversely, differentiated hESCs were no longer highly sensitive to CPT. This attenuated apoptotic response was accompanied by changes in cell cycle profile and by the presence of $p21^{Waf1}$. The results presented here suggest that p53 has a key involvement in preventing the propagation of damaged hESCs when genome is threatened. As a whole, our findings support the concept that the phenomenon of apoptosis is a prominent player in normal embryonic development.

* Corresponding author.
E-mail addresses: carolinapaolagarcia@gmail.com (C.P. García), willyvidelar@hotmail.com (G.A. Videla Richardson), leonardoromorini@gmail.com (L. Romorini), smiriuka@fleni.org.ar (S.G. Miriuka), gsevlever@fleni.org.ar (G.E. Sevlever), mescassa@fleni.org.ar (M.E. Scassa).
[1] Carolina Paola García and Guillermo Agustín Videla Richardson contributed equally to this work.

Introduction

Human embryonic stem cells (hESCs) are a unique cell population derived from the inner cell mass of blastocyst stage embryos (Thomson et al., 1998). These unique cells possess an unlimited potential to proliferate (self-renewal) and the ability to generate and differentiate into most cell

1873-5061
http://dx.doi.org/10.1016/j.scr.2013.12.002

types (pluripotency) (Pera et al., 2000). As such, hESCs should have a highly sensitive and finely tuned response to DNA damage to protect its genome integrity and avoid proliferative defects that may cause lethality. Furthermore, unrepaired or misrepaired DNA lesions can lead to mutations and large scale genome alterations that may compromise cell lineages and affect the well-being of subsequent generations of hESCs. Conversely, somatic cells have genomic requirements that are very different from those of ESCs. Somatic cells have restricted patterns of gene expression characteristic of their specific differentiated lineages. Hence, the consequences of mutation in a somatic cell are limited to that particular cell lineage and may result in somatic diseases, e.g., cancer, but will not be passed on to the progeny.

Camptothecin (CPT) is a highly selective topoisomerase I inhibitor (Liu et al., 2000; Pommier and Cherfils, 2005). This reagent converts topoisomerase I, an essential enzyme in higher eukaryotes, to a cellular poison when replication forks collide with CPT-trapped topoisomerase I cleavage complexes (Pommier, 2006). The resulting lesions are replication-mediated DNA double-strand breaks (DSBs) (Strumberg et al., 2000).

A common step following replication-mediated DSBs is the activation of sensor kinases belonging to the family of phosphatidylinositol 3-kinase-related kinases (PIKKs) (Abraham, 2004). In somatic cells, three PIKKs are activated by topoisomerase I-induced replication mediated DSBs: ataxia teleangectasia mutated (ATM), ataxia teleangectasia mutated and Rad3 related (ATR), and DNA-dependent protein kinase catalytic subunit (DNA-PKcs) (Rao et al., 2005; Ward and Chen, 2001). ATM, ATR and DNA-PKcs activate the DSB signaling pathways by phosphorylating a range of nuclear proteins, which includes histone H2A variant H2AX and p53 (Sordet et al., 2009; Zhao et al., 2008). Phosphorylation of histone H2AX on serine 139 generates γH2AX, a sensitive and early marker for DSBs (Sedelnikova et al., 2003). The formation and resolution of γH2AX is linked to the presence of DSBs and can act as a surrogate for DNA damage and DSB repair. On the other hand, phosphorylation of p53 on serine 15 promotes its activation and fine-tunes its response to DNA damage (Adams et al., 2010).

p53 is a representative tumor suppressor which plays an important role in the regulation of the DNA damage response. In somatic cells, under normal physiological conditions, p53 expression levels and half-life are low. In response to a variety of cellular stressors, p53 is quickly induced and accumulates in cell nucleus. Upon severe DNA damage, p53 induces apoptosis to eliminate damaged cells. Apoptosis induction by p53 can occur via both transcription-dependent and transcription-independent pathways. The classical transcription-dependent pathway involves stabilization of p53 protein via post-translational modifications, nuclear translocation, and subsequent transactivation of pro-apoptotic genes, such as PUMA, Noxa and Bax (Oren, 2003), as well as repression of anti-apoptotic genes such as Bcl-2 and IAPs (Lu, 2005). p53 can also trigger apoptosis via a transcription-independent pathway that involves rapid translocation of a proportion of total cellular p53 directly to the mitochondria and its interaction with the Bcl-2 family members (Chipuk et al., 2004). Conversely, when cells receive repairable DNA damage, p53 promotes cell cycle arrest by transactivating the cyclin dependent kinase inhibitor (CKI) $p21^{Wa'f1}$ to allow DNA repair (Oren, 2003).

Embryonic stem cells progress rapidly through the cell cycle with an unusually short G1 phase (Becker et al., 2006). This unusual cell cycle structure is accompanied by high levels of cyclin-dependent kinase (CDK) activity which is a consequence of the absence or very weak expression of CKIs (Kapinas et al., 2013). Importantly, molecular pathways governing the G1/S transition also play key roles in the DNA damage response and maintenance of genome integrity. In this sense, as hESCs differentiate, the cell cycle structure is remodeled with the G1 phase being markedly lengthened (Filipczyk et al., 2007). These changes in cell cycle dynamics are paralleled by a robust up-regulation of CKIs' mRNA and protein levels.

In this study, we investigated the response of hESCs to the induction of DNA replication stress triggered by CPT. We find that hESCs exhibit high apoptosis rates in response to CPT. Using diverse biochemical and cellular approaches, we determined that DNA-damaged hESCs have functional ATM and DNA-PKcs pathways. Additionally, we present evidence that these PI3KK family members jointly contribute to H2AX phosphorylation, and that CPT treatment leads to p53 stabilization, serine 15 phosphorylation and nuclear accumulation. Importantly, the impairment of p53 translocation to mitochondria with pifithrin-μ ameliorates cell death. The massive apoptosis of hESCs occurs in the absence of $p21^{Waf1}$ protein, despite a marked up-regulation of $p21^{Waf1}$ mRNA levels. Finally, we determined that hESCs at day 14 of the differentiation onset are much less sensitive to CPT than their undifferentiated counterparts. This increase in cell viability is accompanied by p53 stabilization and $p21^{Waf1}$ mRNA and protein induction, concomitantly with a marked decrease in the percentage of cells residing in the S phase. The results presented here prompted us to hypothesize that in hESCs the proapoptotic activity of p53 might prevail to safeguard genome integrity in response to DNA damage.

Materials and methods

Cell culture

The human embryonic stem cell (hESC) line, WA09 (H9), was purchased from WiCell Research Institute (WI) and the hESC line, HUES-5 (H5) was acquired from Harvard University and the Howard Hughes Medical Institute (MA) at low passages (p15 to p20). The hESC lines were maintained on a mitotically inactive (via irradiation) mouse embryonic fibroblast (iMEF) feeder layer in medium comprised of Dulbecco's Modified Eagle's Medium/Ham's F12 (DMEM/F12) supplemented with 20% knockout serum replacement (KSR), 2 mM non-essential amino acids, 2 mM L-glutamine, 100 U/ml penicillin, 50 μg/ml streptomycin, 0.1 mM β-mercaptoethanol and 4 ng/ml of bFGF. All these reagents were obtained from Invitrogen (Carlsbad, CA, USA). For the experiments, hESCs were transferred with 1 mg/ml collagenase IV (Invitrogen, CA, USA) into feeder-free diluted (1/40) Matrigel™ (BD Bioscience, San Jose, CA, USA) coated dishes containing iMEF conditioned medium. For conditioning medium, 3×10^6 inactivated MEFs were incubated for 24 h with 25 ml of DMEM/F12 medium supplemented with 5% KSR and 2 ng/ml of bFGF (in addition to the other aforementioned supplements) and stored at −20 °C. After thawing, fresh aliquots

of KSR and bFGF were added to the medium to render a final concentration of 20% and 4 ng/ml respectively.

To induce differentiation, hESC colonies were treated with 1 mg/ml collagenase type IV (Invitrogen, Carlsbad, CA, USA) for 5 min, followed by mechanical scraping. The dissociated small clumps were then transferred to non-adherent Petri dishes and cultured in DMEM supplemented with 20% (vol/vol) fetal bovine serum (Gibco, CA, USA), 2 mM L-glutamine, 100 U/ml penicillin and 50 μg/ml streptomycin, used as a differentiation medium. The cells were incubated in suspension at 37 °C with 5% CO_2 for 7 days. During the incubation, the suspended hESC clumps aggregated to form three-dimensional non-adherent embryoid bodies (EBs), which were then plated onto 0.1% gelatin coated 24-well microplates and cultured for an additional 7 days.

Human foreskin fibroblasts were prepared as primary cultures from freshly obtained human foreskins as soon as possible after surgery. Written informed consent was obtained from patients according to guidelines established by the Ethics Committee of our institution. Briefly, after fat and loose fascia removal, surgically discarded tissue was trimmed into strips (approximately 0.5 cm × 1.5 cm) using a sterile scalpel. The cut tissue was subjected to an overnight digestion with dispase (Invitrogen, CA, USA) and then followed by careful removal of the epidermis. The remaining dermis was placed in high glucose DMEM, 10% FBS (vol/vol), plated onto tissue culture plates and incubated in a 37 °C, 5% CO_2, 90% humidity incubator. Within 7–10 days outgrowths of fibroblasts appeared. The isolated fibroblasts were then expanded, frozen and stored as described elsewhere.

Inhibitors

2-Morpholin-4-yl-6-thianthren-1-yl-pyran-4-one (KU55933) (Calbiochem, San Diego, CA, USA), (2-(morpholin-4-yl)-benzo [h]chomen-4-one) (NU7026) and pifithrin-μ (Sigma, St. Louis, MO, USA) were dissolved in DMSO and stored at −20 °C. Inhibitors were added to cell cultures such that the final DMSO concentrations were kept constant at 0.25% (v/v). Stock solutions of caffeine were prepared as 100 mM in PBS (Sigma, St. Louis, MO, USA).

Immunostaining and fluorescence microscopy

The hESCs were analyzed for in situ immunofluorescence. Briefly, the cells were rinsed with ice-cold PBS and fixed in PBSA (PBS with 0.1% bovine serum albumin) with 4% formaldehyde for 45 min. After two washes, cells were permeabilized with 0.1% Triton X-100 in PBSA with 10% normal goat serum for 30 min, washed twice and stained with the corresponding primary antibodies. Fluorescent secondary antibodies were used to localize the antigen/primary antibody complexes. The cells were counterstained with DAPI and examined under a Nikon Eclipse TE2000-S inverted microscope equipped with a 20× E-Plan objective and a super high-pressure mercury lamp. The images were acquired with a Nikon DXN1200F digital camera, which was controlled by the EclipseNet software (version 1.20.0 build 61). The following primary antibodies were used: anti-Oct-3/4 (clone C-10) (sc-5279), anti-PARP (sc-8007) (Santa Cruz Biotechnology, Santa Cruz, CA, USA), anti-active Caspase-3 (ab13847), this antibody preferentially recognizes the 17 kDa fragment of the active Caspase-3 (Romorini et al., 2012), anti-pATM (ab81292), anti-γH2AX (ab2893), anti-p53 (ab1101), anti-p73[EP436Y] (ab40658), anti-pSer2056DNA-PKcs (ab181192) (Abcam Inc., Cambridge, MA, USA) and anti-pSer15p53 (cat. 9284) (Cell Signaling Technology, Beverly, MA, USA).

Western blotting

Cells were lysed in ice-cold RIPA buffer supplemented with a protease inhibitor mixture, and protein concentration was determined using the Bicinchoninic Acid Protein Assay (Pierce™, Rockford, IL, USA). Equal amounts of protein were run on 12% polyacrylamide gel electrophoresis, and transferred to PVDF-FL membrane (Millipore, Billerica, MA, USA). The membrane was blocked for 1 h in Odyssey blocking buffer (LI-COR Biosciences, Lincoln, NE, USA) containing 0.1% Tween 20 and then incubated overnight at 4 °C in a solution containing Odyssey blocking buffer, 0.05% Tween 20 and the corresponding primary antibodies. The membrane was washed 4 times for 5 min with TBS containing 0.1% Tween 20 (TTBS), then incubated for 1 h in a

Figure 1 Cell death induced by CPT in hESC line WA09 (H9). (A) H9 cells and human foreskin fibroblasts (HFs) were treated or not with increasing concentrations of CPT (0.1–10 μM) over a 3 h period. Cell viability was measured by the XTT/PMS vital dye assay at 6 or 12 h after drug removal. Results are presented as the percentage of the viability of untreated cells. Each bar represents the mean ± SEM of three independent experiments performed in quintuplicates. A paired Student's *t* test was used to compare CPT treated samples to untreated controls (*$P < 0.05$). (B) Cell cycle distribution of asynchronously growing H9 determined by flow cytometry analysis based on DNA content. (C) Representative images of H9 colonies grown on Matrigel™ coated surfaces for 3 days and treated or not with 1 μM CPT over a 3 h period (left panel); histogram shows quantitative percentage of viable cells assessed by Trypan blue exclusion method 6 h post CPT removal (middle panel); after CPT treatment cells were harvested, and DNA oligomers were quantified by immunoassay (right panel). Results are presented as the percentage of DNA oligomers of untreated cells. Each bar represents the mean ± SEM of three independent experiments performed in triplicates (right panel). A paired Student's *t* test was used to compare CPT treated samples to untreated controls (*$P < 0.05$). (D) Immunofluorescence staining of CPT-treated (1 μM) or untreated H9 cells. The figure shows hESCs stained with primary antibodies against cleaved-caspase-3 recognizing 17 kDa fragment and PARP-1. The nuclei were counterstained with DAPI. Photos were captured at different time points: immediately after CPT treatment (3 h), or 6 h post CPT removal (3 + 6 h). The scale bars represent 100 μm. Representative images and 200% magnifications are shown. (E) Time course of caspase-9 and PARP cleavage in hESCs upon CPT treatment was analyzed by Western blotting with anti-caspase-9 and anti-PARP specific antibodies, immediately after (3 h), 6 or 12 h post drug removal (3 + 6, 3 + 12, respectively). Actin was used as loading control.

solution containing Odyssey blocking buffer, 0.2% Tween 20, and IR-Dye secondary antibodies (1:20.000, LI-COR Biosciences, Lincoln, NE, USA) and subsequently washed 4 times for 5 min in TTBS, and then 1 time for 5 min in TBS. The membrane was immediately scanned for protein bands using the 680 nm and 780 nm channels at a scanning intensity of 4. Immunocomplexes were visualized using the Odyssey Infrared Imaging System (LI-COR). The following primary antibodies were used: anti-Actin (sc-1616), anti-caspase-9 (cat. 9502) (Cell Signaling Technology, Beverly, MA, USA), anti-PARP, that recognizes the C terminus of PARP-1 (sc-8007) (Santa Cruz Biotechnology, Santa Cruz, CA, USA), anti-p27^{Kip1} (clone C-1) (sc-528) (Santa Cruz, CA, USA), anti-p53 (ab1101), anti-p73[EP436Y] (ab40658) (Abcam Inc., Cambridge, MA, USA), anti-pSer15p53 (cat. 9284)

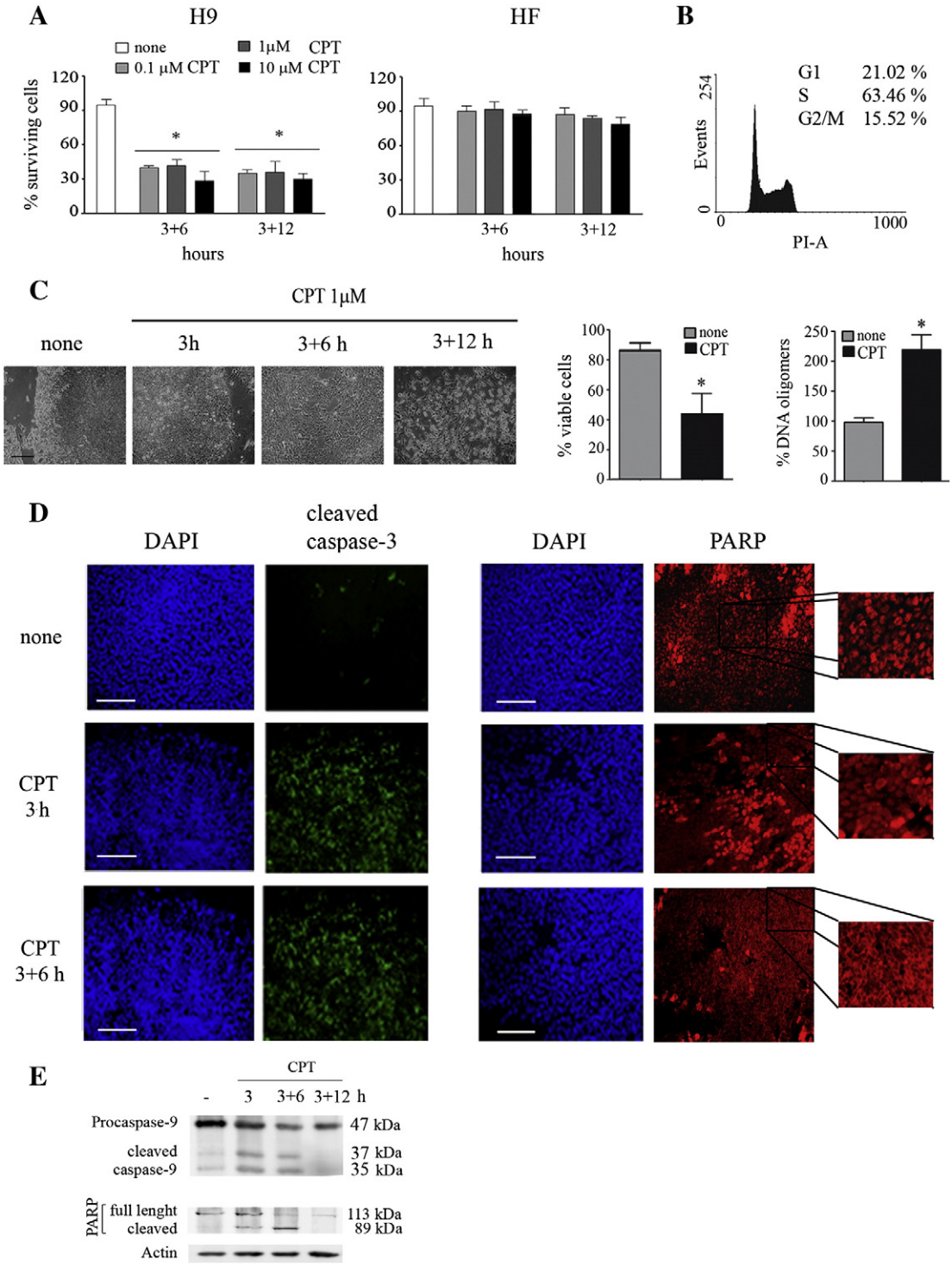

(Cell Signaling Technology, Beverly, MA, USA) and anti-p21^{Waf1} (cat. 556430) (BD Pharmingen™, Becton-Dickinson, San Jose, California, USA). Antigen/primary antibody complexes were detected with near infrared-fluorescence-labeled, IR-Dye 800CW or IR-Dye 680RD, secondary antibodies (LI-COR Biosciences, Lincoln, NE, USA).

Reverse transcription polymerase chain reaction

Total RNA was extracted using TRIzol reagent (Invitrogen, Carlsbad, CA, USA) according to manufacturer's instructions. cDNA was synthesized using MMLV reverse transcriptase (Promega, Madison, WI, USA) from 500 ng of total RNA. The cDNA samples were diluted fivefold. Quantitative PCR studies were carried out using SYBR® Green-ER™ qPCR SuperMix UDG (Invitrogen, Carlsbad, CA, USA) and the primer sequences used are detailed in Supplementary Table 1. All samples were analyzed using an ABI PRISM 7500 Sequence Detector System (Applied Biosystems, Foster City, CA, USA) and were normalized to GAPDH gene expression.

Flow cytometry analysis of cell cycle distribution

Single-cell suspensions of H9 cells were obtained by treatment with acutasse 1× (Invitrogen, CA, USA) (37 °C for 5–10 min). Floating cells were collected, pelleted and washed twice with PBS. For DNA content analysis, cells were fixed in 70% ethanol, rehydrated in PBS, and treated for 30 min with RNase A (1 mg/ml) and for 5 min with propidium iodide (PI) (1 mg/ml). Fluorescence intensity was determined by flow cytometry on a FACScan equipped with a 488-nm argon laser (Becton, Dickinson and Company, Franklin Lakes, NJ, USA). Data acquisition was performed with the CellQuest (Becton, Dickinson and Company, NJ, USA) software, and the percentages of G1, S, and G27M-phase cells were calculated with the MODFIT-*LT* software program (Verity Software House, Topsham, ME, USA). For synchronization, hESCs were blocked with 100 ng/ml nocodazol (Sigma, St. Louis, MO, USA) over a 16 h period. Then, the cells were harvested and analyzed by flow cytometry for cell cycle distribution as described above.

Cell viability assay

hESCs were plated onto Matrigel™ coated 96-well tissue culture plates at densities between 1×10^4 and 3×10^4 cells per well and grown until confluence. A comparable number of EBs were adhered on gelatin coated 48-well plates at day 7, and grown until day 14 of differentiation. At the indicated time points post CPT removal, 50 μg/well of activated 2,3-bis (2-methoxy-4-nitro-5-sulfophenyl)-5 [(phenylamino) carbonyl]-2H-tetrazolium hydroxide (XTT) (Sigma, St. Louis, MO, USA) in PBS containing 0.3 μg/well of the intermediate electron carrier, N-methyl dibenzopyrazine methyl sulfate (PMS) (Sigma, St. Louis, MO, USA) was added (final volume 100 μl) and incubated for 2–3 h at 37 °C. Cellular metabolic activity was determined by measuring the absorbance of the samples with a multiplate spectrophotometer (Benchmark, Bio-Rad, Hercules, CA, USA) at a wavelength of 450 nm and subtracting the background absorbance at 690 nm.

Trypan blue staining

For Trypan blue exclusion assay, cells were seeded in 6-well plates at a density of 1×10^5 cells/ml. At the indicated time points after treatment, both the adherent and detached cells were collected and stained with 0.4% Trypan blue solution (final concentration 0.08%) (Sigma, St. Louis, MO, USA) for 5 min at room temperature. Cells stained blue (dead) and unstained (live) were counted in a hemocytometer chamber. Percentages of viable cells were calculated as total number of live cells divided by total number of cells and multiplied by 100.

Flow cytometric determination of apoptosis by Annexin V/propidium iodide double staining

FITC-Annexin V Apoptosis Detection Kit I was used to measure cell death by flow cytometry according to the manufacturer's instructions (BD Bioscience, Heidelberg, Germany). Briefly, following two washing steps with PBS, the cell pellets were re-suspended in 1× Binding Buffer (0.01 M HEPES pH 7.4, 0.14 M NaCl and 2.5 mM $CaCl_2$) at a concentration of 1×10^6 cells/ml. Each sample (100 μl of the solution, 1×10^5 cells) was transferred to a tube and was stained by addition of 5 μl annexin V-FITC and 5 μl propidium iodide. After incubation in the dark for 15 min at room temperature, 400 μl of 1× Binding Buffer was added to each tube and cell suspensions were analyzed by flow cytometry within 1 h. Data was acquired on a BD Accuri C6 flow cytometer using BD Accuri C6 software.

Assessment of DNA fragmentation

CPT-induced apoptosis was quantified by direct determination of nucleosomal DNA fragmentation with Cell Death Detection ELISA^{Plus} kit (Roche, Mannheim, Germany). This assay uses specific monoclonal antibodies directed against histones from fragmented DNA, allowing the determination of mono and oligonucleosomes in the cytoplasmic fraction of cell lysates. Briefly, 2×10^5 hESCs were plated on 24-well plates in 500 μl culture medium. Three hours after CPT addition (1 μM), cells were lysed according to the manufacturer's manual, followed by centrifugation (200 ×*g*, 5 min). Alternatively, pifithrin-μ (10 μM) was added to the medium 1 h before and during treatment with CPT. The mono and oligonucleosomes in the supernatants were determined using an anti-histone-biotin antibody. The resulting color development, which was proportional to the amount of nucleosomes captured in the antibody sandwich, was measured at 405 nm wavelength using a Benchmark microtiter plate reader (Bio-Rad Hercules, CA, USA). Results were expressed as DNA oligomer percentage, calculated from the ratio of absorbance of treated samples to that of the untreated ones.

Statistical analysis

All results are expressed as the mean ± SEM. The Student's paired *t*-test was used to determine significant differences between means, and P values below 0.05 were considered to be statistically significant.

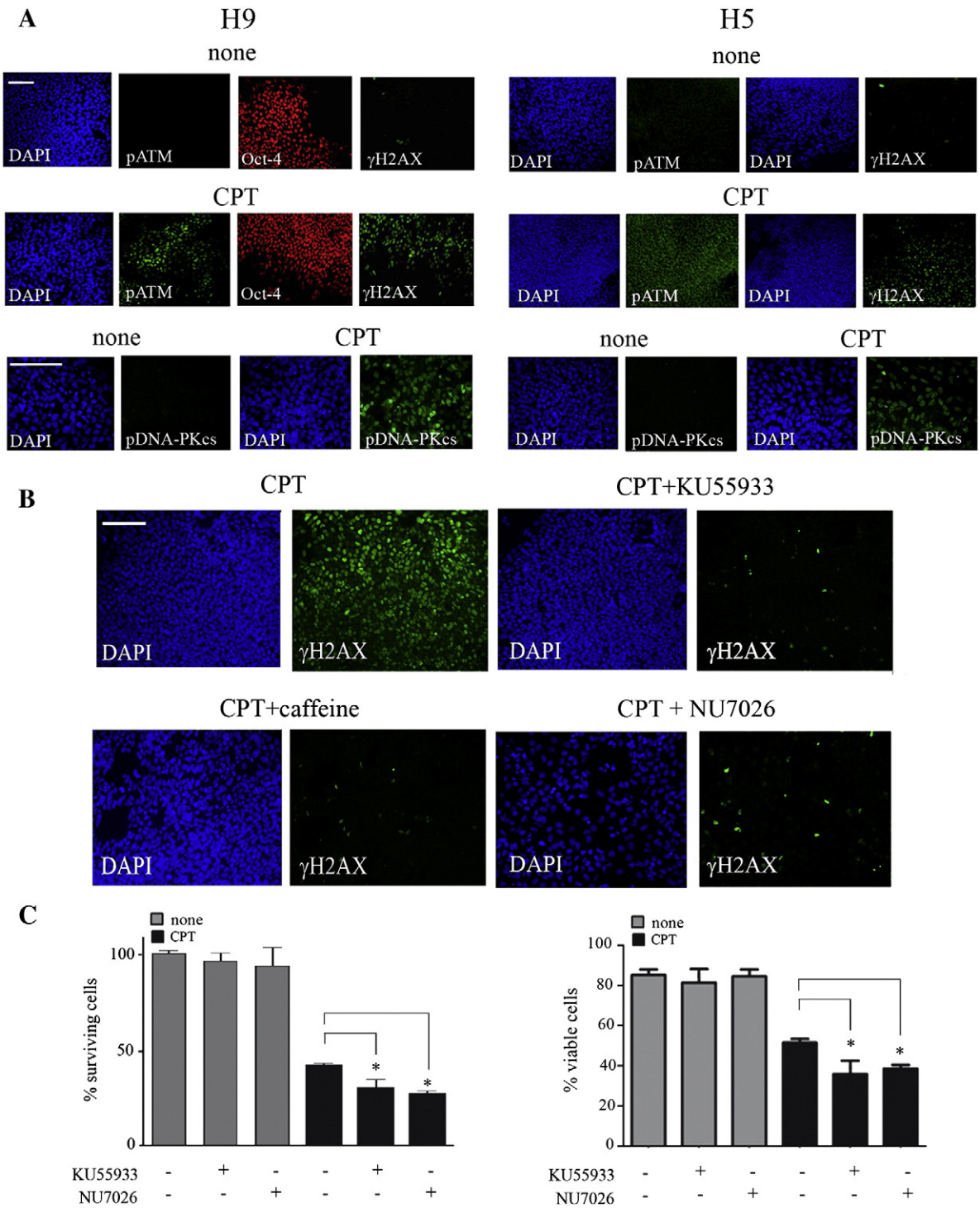

Figure 2 DNA-damage signaling in CPT exposed hESCs. (A): Immunofluorescence staining of CPT-treated (1 μM over a 3 h period) or untreated H9 and H5 cells. The figure shows representative images of hESCs stained with primary antibodies against ATM phospho-serine 1981 (pATM), Oct-4, a key factor that governs pluripotency and self-renewal in hESCs, histone H2AX phospho-serine 139 (γH2AX) and DNA-PKcs phospho-serine 2056 (pDNA-PKcs). (B) Fluorescent immunoreactivity of γH2AX in H9 pretreated with 100 μM KU55933, 10 mM caffeine or 50 μM NU7026 for 1 h and exposed to 1 μM CPT for 3 h. The scale bars represent 100 μm. (C) H9 cells were pretreated with KU55933 (100 μM) or NU7026 (50 μM) 1 h and during CPT exposure (1 μM over a 3 h period). Cell viability was measured by the XTT/PMS vital dye assay at 6 h after drug removal. Results are presented as the percentage of the viability of untreated cells. Histogram shows quantitative percentage of viable cells assessed by Trypan blue exclusion method 6 h post CPT removal. Each bar represents the mean ± SEM of three independent experiments performed in quintuplicates. A paired Student's *t* test was used to compare samples in the presence or absence of each inhibitor (*$P < 0.05$).

Results

CPT promotes apoptosis in hESCs

First, we evaluated the effect of CPT on WA09 (H9) hESC viability. To do so, we determined the percentage of surviving cells at different time points post CPT removal using a XTT/PMS vital dye assay. The percentage of surviving cells decreased to approximately 40% as soon as 6 h and further after genotoxic removal. Viability was significantly reduced to the same extent when hESCs were exposed to CPT during 3 h at concentrations ranging from 0.1 to 10 μM (Fig. 1A). Similar results were obtained when live and dead cells were counted using Trypan blue dye-exclusion assay. As shown in Fig. 1C (middle panel) the percentage of viable cells markedly decrease 6 h after drug removal. Conversely, the number of viable human primary foreskin fibroblasts (HF) slightly decreased to 80% after a withdrawal period of 12 h, when cultured for 3 h in the presence of 10 μM CPT (Fig. 1A). Interestingly, we determined that 10–15% of H9 cells grown on Matrigel coated surfaces were undergoing spontaneous cell death (Fig. 1C, middle panel).

With some exceptions, hESCs divide rapidly with generation times of 8–16 h. H9 cells were synchronized at the G2 phase with nocodazole (100 ng/ml, 16 h) (Supplementary Fig. 1A) and then were analyzed for cell cycle position every 3 h after drug removal by flow cytometry (data not shown). In accordance with previous data (Becker et al., 2006), we determined that the total time required for cell division of these pluripotent cells is 16 ± 0.5 h, with an estimated time for G_1 of approximately 2.5–3 h, an S phase of 8 h and a combined period of G_2/M of 5 h. Thus, at any given time, almost 60–65% of hESCs reside in S phase (Fig. 1B). This may explain, at least in part, the high decrease in cell viability observed upon CPT treatment especially if we consider that the primary mechanism by which CPT kills cells is through S phase specific cytotoxicity. Moreover, damaged H9 cells exhibited a progressive ballooning, shrinking and detachment from Matrigel™ coated surfaces (Fig. 1C, left panel). These morphological changes are suggestive of apoptotic processes.

Phosphatidylserine (PS) translocation from the inner to the outer leaflet of the plasma membrane has been considered a characteristic feature of apoptosis. So, to determine if CPT induces apoptosis in H9 cells, we examined PS exposure and plasma membrane integrity simultaneously by annexin V (a phospholipid-binding protein with high affinity for PS) and propidium iodide (PI) double staining. Importantly, PI can only penetrate the plasma membrane when membrane integrity is breached, as occurs in the later stages of apoptosis or in necrosis. So, in this assay, apoptotic cells are positive for annexin V but negative for PI. By flow cytometry analysis, we detected an increased number of annexin V^+/PI^- cells after CPT exposure, concomitant with a decrease in the number of live cells (annexin V^-/PI^-). The number of annexin V^+/PI^+ cells remained less than 10% during the timeframe of the experiments (Supplementary Fig. 1D). Moreover, CPT-induced cell death in H9 cells was accompanied by a significant increase in the percentage of subG_1 cells with a subdiploid DNA content indicating DNA degradation (Supplementary Fig. 1C).

The uniform degradation of genomic DNA into oligomers of approximately 180–200 bp, or multiples of that, characterizes inter-nucleosomal cleavage of DNA and constitutes a biochemical hallmark of apoptosis. Thus, to investigate whether the loss of cell viability was due to CPT-induced apoptosis, we determined cell death levels of treated and untreated H9 hESCs by quantifying DNA oligomers with an enzyme-linked immunosorbent assay (ELISA), using monoclonal antibodies directed against DNA and histones. As shown in Fig. 1C (right panel) a marked increase in the percentage of DNA oligomers was observed immediately after CPT removal (1 μM, 3 h) in H9 damaged cells.

Many apoptotic triggers culminate in the activation of caspase cascades. Thus, to evaluate whether topoisomerase I inhibition leads to caspase activation in H9 cells, we performed Western blot analysis and find that 3 h after CPT treatment, initiator pro-caspase-9 (47 kDa) was processed into active fragments (37/35 kDa) (Fig. 1E). Cleaved caspase-9 could further process other caspase members, including caspase-3.

Next, to gain further insight into the apoptotic events triggered by CPT, we stained cell colonies with cleaved caspase-3 antibody (early marker for apoptosis) to determine if this effector caspase was activated. Intense immunoreactivity was observed 3 h after CPT addition (Fig. 1D). Active executioner caspase-3 can further cleave downstream substrates involved in apoptotic changes such as poly-(ADP-ribose) polymerase (PARP). Time course assays revealed the presence of cleaved PARP as early as 3 h after CPT addition and onwards (Fig. 1E). Earlier studies suggest that caspase-cleaved PARP translocates to the cytoplasm during apoptosis (Ang et al., 2003). As shown in Fig. 1D (bottom panel) cytosolic PARP could be seen 6 h after CPT withdrawal. PARP translocation was

Figure 3 CPT triggers p53 stabilization and phosphorylation at Serine 15 in H9 cells. (A) Time course of p53 stabilization and phosphorylation at serine 15 in hESCs upon CPT treatment was analyzed by Western blotting with anti-p53 and anti-p53phospho-serine 15 (p53pSer15) specific antibodies, immediately after (3 h), 6 or 12 h post drug removal (3 + 6, 3 + 12, respectively). Actin was used as loading control. (B) Immunofluorescence staining of CPT-treated (1 μM) or untreated H9 cells. The figure shows representative images of hESCs stained with primary antibodies against p53, p53pSer15 and p73 (transactivation domain). The nuclei were counterstained with DAPI. Photos were captured immediately after CPT treatment (1.5 or 3 h). The scale bars represent 100 μm. (C) Fluorescent immunoreactivity of p53pSer15 in H9 cells pretreated with 100 μM KU55933 or 10 mM caffeine for 1 h and exposed to 1 μM CPT for 3 h. The scale bars represent 50 μm. (D) After CPT treatment (1 μM over a 3 h period) cells were harvested, and DNA oligomer levels were measured by immunoassay. Results are presented as the percentage of DNA oligomers of untreated cells. Each bar represents the mean ± SEM of three independent experiments performed in triplicates (left panel). Cell viability was measured by the XTT/PMS vital dye assay at 6 h after drug removal in PFT-μ treated or untreated cells (10 μM, 1 h before and during CPT exposure). Results are presented as the percentage of the viability of untreated cells (middle panel). Histogram shows quantitative percentage of viable cells assessed by Trypan blue exclusion method 6 h post CPT removal in PFT-μ treated or untreated cells (right panel). Each bar represents the mean ± SEM of three independent experiments performed in quintuplicates. In all cases, a paired Student's *t* test was used to compare CPT plus PFT-μ treated samples to CPT treated ones (*$P < 0.05$).

preceded by the appearance of catalytically active caspase-3. This chronology is compatible with the involvement of caspase-3 in PARP proteolysis.

DNA damage-response signaling in CPT-treated hESCs

DNA topoisomerase I inhibitors exert their cytotoxic effects in replicating cells by inducing DSBs (Arnaudeau et al., 2001). The induction of a wide range of cellular responses to DSBs depends mainly on a functional ATM (Rotman and Shiloh, 1999). Upon diverse genotoxic stress, ATM is recruited to the sites of DSBs, where it becomes activated through autophosphorylation at serine 1981 (Kobayashi et al., 2009). We investigated ATM phosphorylation at this residue in H9 and HUES-5 (H5) cells by fluorescent immunocytochemistry. As seen in Fig. 2A, phosphorylation of ATM at serine 1981 was evident in hESC nuclei 3 h after 1 μM CPT exposure.

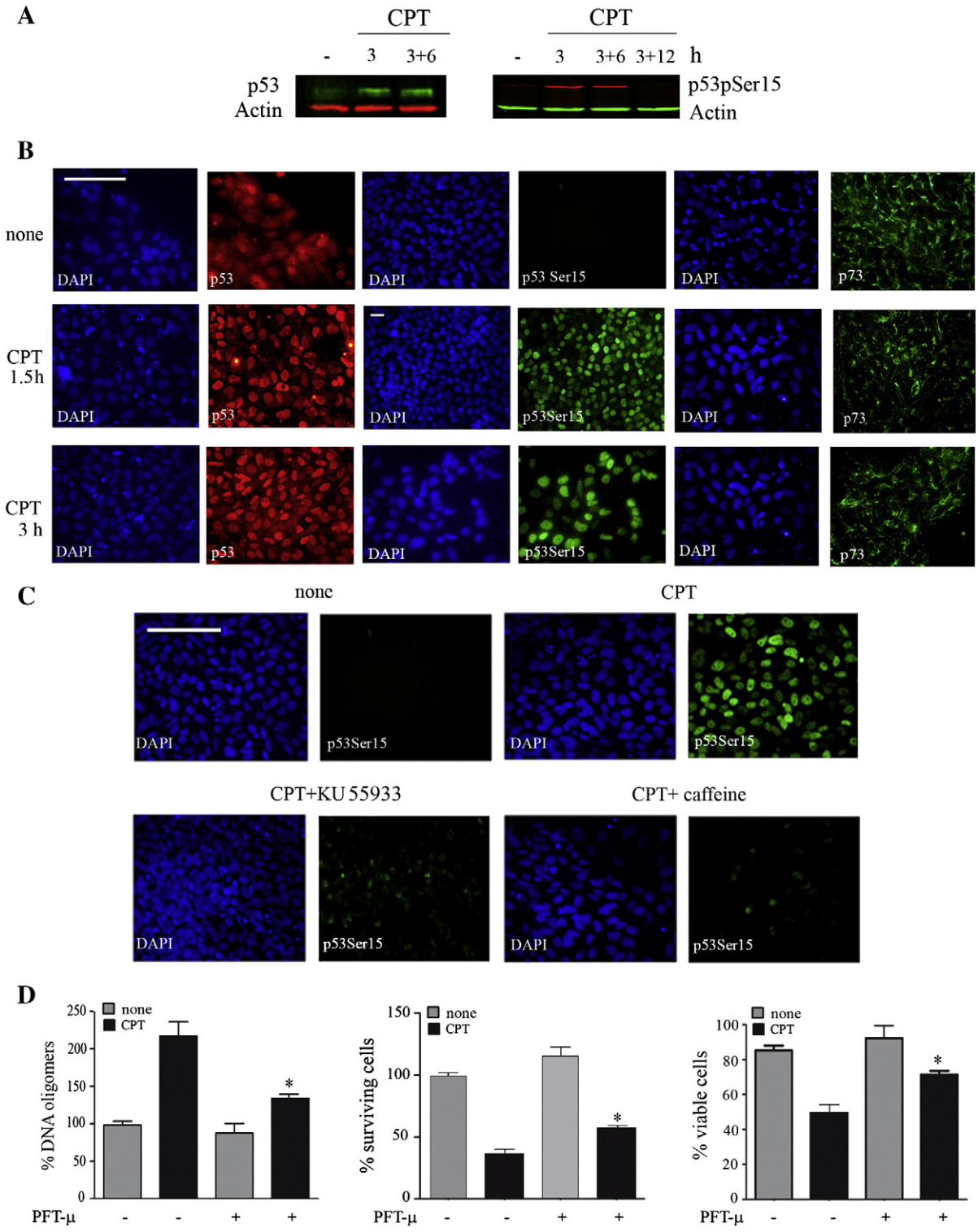

Several studies show that, rather than overlapping, the roles of ATM and DNA-PKcs in DSBs repair can be described as complementary, since the presence of the two kinases is absolutely necessary in order to avoid faulty DSBs rejoining and achieve legitimate repair (Martin et al., 2012). It has been reported that CPT treatment induces DNA-PKcs phosphorylation at serine 2056 (required for the repair of DSBs) in human skin fibroblasts. Importantly, serine 2056 phosphorylation was associated with replication fork progression and occurred only in cells synchronized in the S phase, suggesting that DNA replication-associated DSBs activate DNA-PKcs (Chen et al., 2005). To determine if CPT exposure leads to DNA-PKcs phosphorylation in hESCs, we immunostained cells with anti-pSer2056 DNA-PKcs antibody. A high nuclear immunoreactivity was observed in H9 and H5 cells within 3 h of topoisomerase I inhibition (Fig. 2A, bottom panel).

We then evaluated CPT-induced DNA damage response by measuring the activation of ATM downstream target, H2AX (Sordet et al., 2009). High levels of H2AX phosphorylated on serine 139 (γH2AX) were detected in hESCs within 1 h of CPT addition (data not shown) and along treatment (3 h) (Fig. 2A). Interestingly, despite the small decrease in cell viability observed in HF after CPT exposure, the phosphorylation of ATM at serine 1981 and the levels of γH2AX immunoreactivity exhibited by damaged fibroblasts were similar to those seen in hESCs under the same experimental conditions (CPT, 1 μM, 3 h) (Supplementary Fig. 2).

To test whether ATM was responsible for H2AX phosphorylation, we incubated H9 cells with 100 μM ATM-specific inhibitor, KU55933, or 10 mM PI3KK-inhibitor, caffeine; 1 h before and during treatment with the topoisomerase I inhibitor. Consistent with previous data, our dose response experiments revealed that a concentration of 100 μM KU55933 is needed to effectively inhibit ATM signaling in hESCs (Momcilovic et al., 2009). Incubation of hESCs with either of these inhibitors impaired H2AX phosphorylation triggered by genotoxic stress, which was manifested by a pronounced decrease in γH2AX signal intensity (Fig. 2B).

Once activated, DNA-PKcs can phosphorylate a number of substrates including H2AX (An et al., 2010). To assess whether DNA-PKcs contributes to H2AX phosphorylation in hESCs exposed to CPT, we used a selective inhibitor, NU7026 (Callen et al., 2009). DNA-PKcs inhibitor treatment (50 μM) resulted in reduced H2AX phosphorylation (Fig. 2B). In all cases, basal levels of γH2AX were not affected by these inhibitors at the concentrations and periods assayed (data not shown). Collectively, these findings demonstrate that CPT treatment leads to ATM and DNA-PKcs activation and that both PI3KKs jointly contribute to H2AX phosphorylation in hESCs.

The activation of ATM and DNA-PKcs and the subsequent phosphorylation of its downstream targets in response to CPT prompted us to investigate whether the inhibition of these sensor kinases would affect the propensity of hESCs to undergo cell death upon genotoxic stress. To address this issue, we treated hESCs 1 h before and during CPT treatment (1 μM, 3 h) with KU55933 (100 μM) or NU7026 (50 μm) and measured cell viability by XTT and Trypan blue exclusion assays. As seen in Fig. 2C, the impairment of ATM or DNA-PKcs activity further decreased the percentage of viable cells 6 h after CPT removal. The presence of ATM or DNA-PKcs inhibitor did not affect unstressed hESC viability during the timeframe of the experiment (Fig. 2C).

p53 is stabilized and phosphorylated on serine 15 upon CPT exposure in hESCs

As p53 is a major downstream effector of the ATM-mediated response to DNA damage, we next assessed whether

Figure 4 $p21^{Waf1}$ expression upon CPT exposure in undifferentiated and differentiated H9 cells. (A) Analysis of mRNA expression levels by real time RT-PCR in H9 cells and human foreskin fibroblasts (HF) immediately after 1 μM CPT treatment (3 h), 6 h or 12 h post CPT removal (3 + 6 h, 3 + 12 h, respectively) with primers that amplified $p21^{Waf1}$. GAPDH expression was used as normalizer. Graphs show mRNA fold change relative to untreated control cells, arbitrarily set as 1. Bars represent the mean ± SEM of three different experiments performed in duplicate. Student's *t* test was used to compare CPT-treated to untreated samples (*$P < 0.05$). (B) Western blot analysis in H9 cells (right panel) and human foreskin fibroblasts (left panel) immediately after 1 μM CPT treatment (3 h), 6 h or 12 h post CPT removal (3 + 6 h, 3 + 12 h, respectively) using specific antibodies against $p21^{Waf1}$, $p27^{Kip1}$ and Actin (loading control). (C) Effect of hESC differentiation on cell cycle structure. Pluripotent H9 cells were subjected to an embryoid body based differentiation protocol and analyzed by flow cytometry at the indicated time points. DNA histograms of H9 cells (right panel). Immunofluorescence staining of undifferentiated H9 cells (day 0) and EBs (day 14) labeled with Ki67. The nuclei were counterstained with DAPI. The scale bars represent 100 μm (left panel). Analysis of $p27^{Kip1}$ and $p57^{Kip2}$ mRNA levels by real time RT-PCR in undifferentiated H9 cells and EBs at indicated time points along differentiation. Graphs show mRNA fold change relative to undifferentiated control cells at each time point of differentiation, arbitrarily set as 1 for each of analyzed transcript (bottom panel) (D). Analysis of $p21^{Waf1}$ mRNA levels by real time RT-PCR in undifferentiated H9 cells and EBs treated or not with CPT (1 μM over a 3 h period) at indicated time points along differentiation. Graphs show mRNA fold change relative to undifferentiated control cells at each time point of differentiation, arbitrarily set as 1. Bars represent the mean ± SEM of three different experiments performed in duplicate. Student's *t* test was used to compare CPT-treated to untreated samples (*$P < 0.05$). Western blot analysis of EBs derived from H9 cells, unstressed or exposed to CPT, using specific antibodies against p53, p73, $p21^{Waf1}$ and Actin (loading control). (E) H9-derived EBs at day 14 of differentiation were treated or not with increasing concentrations of CPT (1–10 μM) during 3 h. Cell viability was measured by the XTT/PMS vital dye assay at 12 h after drug removal. Results are presented as the percentage of the viability of untreated EBs (left panel). Histogram shows quantitative percentage of viable cells assessed by Trypan blue exclusion method (right panel). Each bar represents the mean ± SEM of three independent experiments performed in quintuplicates. (F) 12 h after CPT withdrawal (1 μM over a 3 h period) EBs (day14) were harvested, and DNA oligomer levels were measured by immunoassay. Results are presented as the percentage of DNA oligomers of untreated EBs. Each bar represents the mean ± SEM of three independent experiments performed in triplicates. In all cases, a paired Student's *t* test was used to compare CPT treated samples to untreated controls (*$P < 0.05$).

topoisomerase I inhibition promotes p53 phosphorylation on serine 15 in pluripotent stem cells. To do so, CPT-treated (1 μM for 3 h) H9 cells were harvested at different time points post-treatment and subjected to Western blot assays. Immunoblot analysis revealed that p53 is stabilized and phosphorylated on serine 15 in response to CPT. Enhanced levels of p53 and phospho-p53(Ser15) were seen following a 3 h treatment with CPT and onwards. p53 phosphorylation declined thereafter and returned to baseline 12 h after drug removal (Fig. 3A).

Immunofluorescence studies showed a diffuse cytosolic and nuclear staining pattern of p53 in untreated H9 hESCs (Fig. 3B). However, upon genotoxic stress, p53 rapidly accumulated in the nucleus and underwent N-terminal phosphorylation at serine 15. This activation occurred within 1.5 h after CPT addition (Fig. 3B). In contrast, p73, a p53 family member, appeared widely distributed throughout the cytoplasm when H9 hESCs were stained with an antibody that recognizes its transactivation domain. CPT treatment did not induce changes in p73 localization at least at the concentrations and time points assayed (Fig. 3B).

To examine whether regulation of p53 protein through post-translational mechanisms was achieved by ATM, we pre-incubated H9 cells with KU55933 (100 μM) or caffeine (10 mM) and exposed them to CPT for 1.5 or 3 h. As shown in Fig. 3C, the presence of ATM inhibitor markedly reduced phospho-p53(Ser15) fluorescent signal. Moreover, caffeine treatment almost completely impaired p53 phosphorylation in CPT-damaged hESCs.

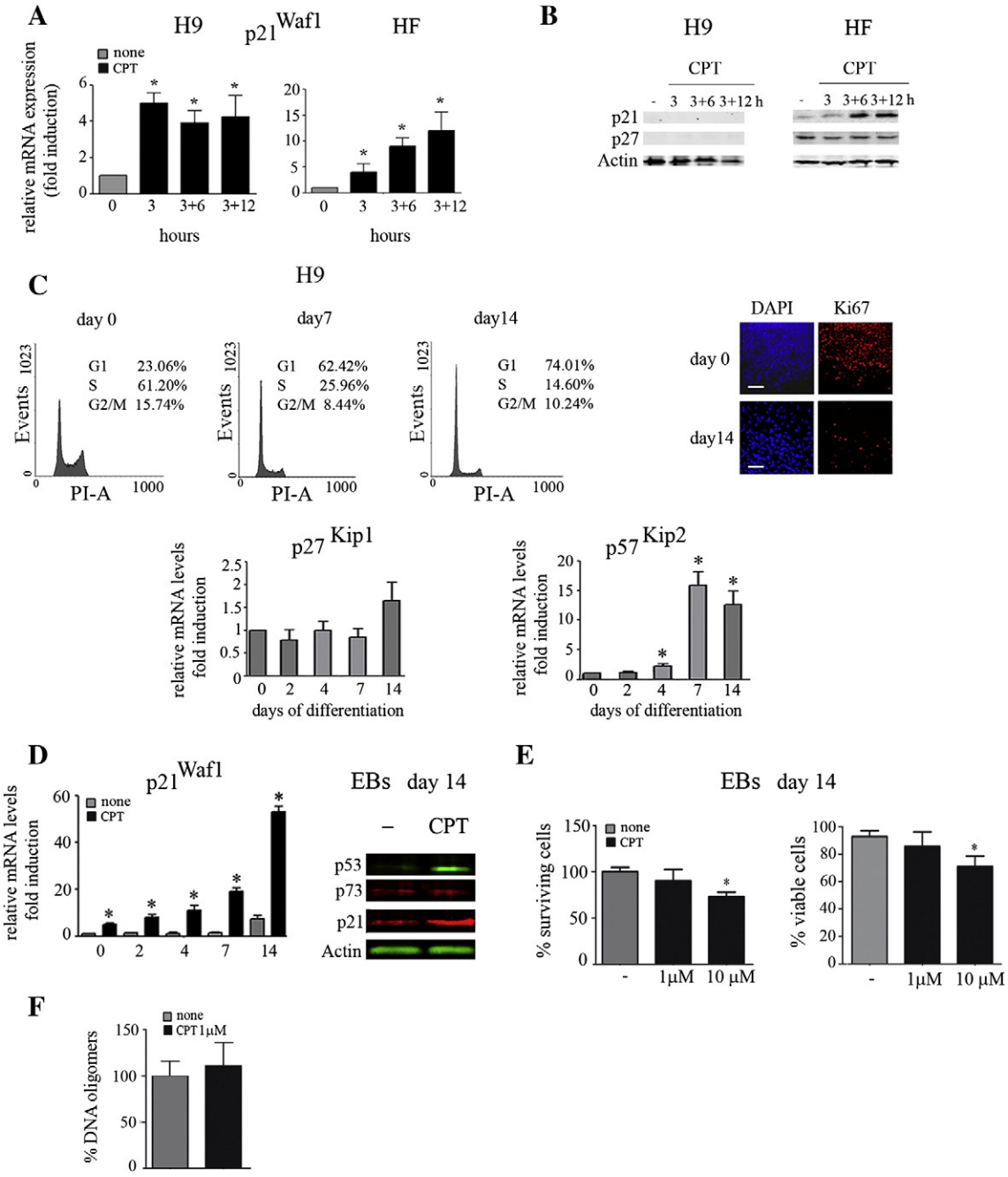

Inhibition of mitochondrial p53 translocation by pifithrin-μ protects hESCs from CPT-induced apoptosis

In many cell types, p53 rapidly mounts a direct mitochondrial death program that precedes transcription-mediated apoptosis in response to intense stress (Vaseva and Moll, 2009). Thus, to test whether this phenomenon was also operative in hESCs, we treated H9 cells with pifithrin-μ (PFT-μ) a small molecule that inhibits p53 binding to mitochondria by reducing its affinity to Bcl-xL and Bcl-2 but has no effect on p53-dependent transactivation (Strom et al., 2006). The aforementioned factors are expressed in H9 cells (Romorini et al., 2012).

First, we determined apoptosis levels of CPT-treated hESCs, in the presence or absence of PFT-μ, by quantifying DNA oligomers. As seen in Fig. 3D, PFT-μ treatment (10 μM) reduced approximately 30% the amount of CPT-induced DNA oligomers in H9 hESCs. Then, to gain insight into the involvement of p53′ mitochondrial program in CPT induced apoptosis we perform cell viability assays in PFT-μ treated or untreated H9 cells. By XTT/PMS vital dye and Trypan blue exclusion assays we determined that cell viability was increased by 27% and 22%, respectively, in PFT-μ treated hESCs suggesting that in this case, p53 is acting as a proapoptotic factor rather than an antiapoptotic one. Interestingly, and according to previous reports (Grandela et al., 2007), we also find that PFT-μ protects cells from spontaneous apoptosis (10 to 15%) (Fig. 3D, middle and right panels). Importantly, H9 cells displayed similar levels of γH2AX immunoreactivity, p53 nuclear accumulation and phosphorylation at serine 15 after CPT exposure, either in the presence or in the absence of the inhibitor (Supplementary Fig. 3).

DNA damage response toward topoisomerase I inhibition is achieved in the absence of cyclin-dependent kinase inhibitor, $p21^{Waf1}$, in undifferentiated hESCs

Depending on the extent of an insult, damaged DNA can initiate a signaling pathway that leads either to cell cycle arrest in which the cell is given the opportunity to repair damaged DNA or to the complete disposal of the cell by apoptosis. One of the main players deciding the cell fate following DNA damage is p53 (Tian et al., 2012). In adult cells, cell cycle arrest induced by p53 is mainly mediated by the Cip/Kip family member, the CKI, $p21^{Waf1}$ (Zhang et al., 2010). The observed phosphorylation of p53 triggered by CPT in hESCs prompted us to investigate $p21^{Waf1}$ expression levels in these cells upon damage. Quantitative RT-PCR analysis revealed a robust induction of $p21^{Waf1}$ mRNA 3 h after 1 μM CPT addition (approximately 5 fold), similar to that observed in HF (Fig. 4A). However, $p21^{Waf1}$ transcript levels were more sustained and strongly induced in fibroblasts than in hESCs after drug withdrawal (Fig. 4A). In damaged HF the increase in $p21^{Waf1}$ mRNA levels was also reflected by changes in the protein levels (Fig. 4B, right panel). Conversely and importantly, both in control and CPT-treated H9 cells, $p21^{Waf1}$ protein levels assessed by Western blotting were undetectable at all tested time points (Fig. 4B, left panel). These observations are in agreement with previous results obtained with several hESC lines upon treatment with different classes of DNA damaging agents (Barta et al., 2010; Filion et al., 2009; Hyka-Nouspikel et al., 2012). Moreover, previous work had demonstrated that multiple microRNAs, specifically expressed in pluripotent cells, target the 3′-UTR of the $p21^{Waf1}$ transcript to down-regulate translation (Wang and Blelloch, 2009).

In addition, $p27^{Kip1}$, another Cip/Kip family member, was also undetectable by immunoblotting in these pluripotent cells (Fig. 4B, left panel). An increasing number of reports describe that active CDKs are required to initiate apoptotic processes, including those induced by genotoxics (Janicke et al., 2007; Yu et al., 2005). Importantly, ESCs exhibit high levels of CDK activity, which are the consequence of the absence or very weak expression of CKIs (Koledova et al., 2010). The unique expression pattern of key cell cycle regulators in hESCs may compose a scenario where genotoxic-induced apoptosis is facilitated and may account for the increased loss in cell viability observed in CPT-damaged H9 cells (Fig. 1A).

$p21^{Waf1}$ protein is induced in response to CPT in differentiated hESCs

In vitro differentiation of hESCs into three-dimensional cell aggregates, called embryoid bodies (EBs), is induced by addition of serum and withdrawal of basic fibroblast growth factor in a feeder-layer free culture. This differentiation process is accompanied by decline in levels of proteins and mRNAs associated with stemness, increased expression of endodermal, ectodermal and mesodermal markers and changes in cell cycle structure and dynamics. During differentiation a decrease in pluripotency-associated gene expression (Oct-4, Nanog), concomitant with an up-regulation of endodermal (GATA-6, alpha fetoprotein), ectodermal (Pax-6), early mesodermal (brachury) and cardiac mesodermal (atrial natriuretic peptide, cardiac troponin T) markers among others, is observed (Scassa et al., 2011).

Different regulatory mechanisms create direct links between cell cycle structure and differentiation stage during development. Consequently, there is no definitive cell cycle but many different cell cycle settings adapted to each stage of differentiation. Thus, to assess differentiation-associated changes in cell cycle profiles, we evaluated the cell cycle structure of undifferentiated hESCs and EBs at day 7 or 14 from differentiation onset. A progressive and sustained increase in the number of cells residing in $G_{0/1}$ phase and a reduction in the percentage of cells transiting S phase was determined as differentiation proceeded by flow cytometry analysis. A strong resemblance between the cell cycle profiles of EBs (14 days) and human foreskin fibroblasts was observed (Supplementary Fig. 1B). We also examined the expression of the proliferation marker, Ki67, in hESCs and EBs. As shown in Fig. 4C (right panel) at the undifferentiated state, all H9 cells stained positively for Ki67 antibody, indicating the absence of quiescent (G_0) cells. Conversely, at day 14 of differentiation an increase in G_0 phase population was evidenced by negative Ki67 labeling. These data correlates with the cell cycle distribution profiles exhibited by proliferating and differentiating cells.

In consonance with these changes, a marked increase in Cip/Kip family members mRNA levels was determined by real time RT-PCR analysis. $p21^{Waf1}$ was robustly induced (7.5 fold) in EBs at day 14 of differentiation (Fig. 4D). Importantly, $p57^{Kip2}$ mRNA level was up-regulated earlier and sustainably from day

7 and onwards (15 fold) (Fig. 4C, bottom panel). This finding is consistent with the specific role that this CKI plays in embryonic development, where substantial and timely changes of $p57^{Kip2}$ are required for accurate differentiation of tissues (Borriello et al., 2011). Conversely, $p27^{Kip1}$ transcript levels did not vary significantly at all time points assayed (Fig. 4C, bottom panel). This correlates with the fact that $p27^{Kip1}$ plays a critical role in the establishment of quiescence and its expression is increased in mitogen-deprived or terminally differentiated cells (Gonzalez et al., 2003). Along differentiation, cells undergo molecular changes that influence their fate. Thus, the up-regulation of CKI levels observed herein can be attributed, at least in part, to the facts that a timely regulated exit from cell cycle is required for proper differentiation and a decrease in CDK activities is necessary to safeguard excessive apoptosis.

We further examined the effect triggered by CPT on $p21^{Waf1}$ mRNA levels at different time points during H9 hESC differentiation. As occur in several cell types, $p21^{Waf1}$ was markedly induced upon genotoxic stress at all stages of differentiation (approximately 7 fold) (Fig. 4D).

Several studies have clearly reported that p53 protein levels increase swiftly in response to DNA damage. In addition, a number of studies have recently shown that the p53 family member, p73, is also up-regulated and activated by diverse genotoxic stresses (Zaika et al., 2011). Here, we sought to determine if these proteins were stabilized in EBs upon CPT treatment. As seen in Fig. 4D (right panel) a robust increase in p53 abundance was visible within 3 h of CPT addition, while p73 protein levels remained unaffected. These findings suggest that, unlike p53, p73 activation seems only to be triggered by a subset of DNA damaging agents.

We next examined whether EBs at day 14 of differentiation express $p21^{Waf1}$ protein and, if this cell cycle inhibitor was induced upon CPT-induced DNA damage. By Western blot analysis we determined that $p21^{Waf1}$ is clearly detectable in unstressed EBs. As expected, the stabilization of p53 following CPT exposure (1 μM, 3 h) was accompanied by a robust induction of $p21^{Waf1}$, a bona fide p53 target gene (Fig. 4D, right panel).

Finally, to assess differentiated hESCs response to CPT, we evaluated cell viability in EBs at day 14 of differentiation in the presence of increasing doses of CPT during 3 h. We find that approximately 91% of EBs survive at 1 μM CPT and 74% of EBs remain viable at 10 μM CPT after a withdrawal period of 12 h (Fig. 4E), resembling the response described for HF (Fig. 1A). Furthermore, we determined the percentage of viable cells using Trypan blue staining. As shown in Fig. 4E (right panel) a slight decrease in the percentage of viable cells (23%) was observed 12 h after CPT removal (10 μM). Remarkably, no significant difference appeared between the amounts of DNA oligomers present in stressed and in unstressed EBs as judged by ELISA quantification (Fig. 4F). Thus, EBs are no longer highly sensitive to CPT even when exposed to a 10-fold higher dose than their differentiated counterparts. Interestingly, the levels of γH2AX immunoreactivity displayed by CPT-treated EBs (1 μM, 3 h) were similar to those seen in damaged hESCs, suggesting that the differential response to genotoxic observed between hESCs and EBs is not the consequence of different extents of DNA damage (Supplementary Fig. 2B). A priori, this attenuated response may be attributed, at least in part, to the marked reduction in the fraction of cells transiting S phase (CPT-susceptible cells), which decreased from approximately 65–60% at day 0 to 15% at day 14 of differentiation (histograms, Fig. 4C).

Discussion

Currently, the mechanisms that protect the genome in rapidly proliferating hESCs are minimally understood. In the present study we demonstrate that H9 and H5 hESC lines respond to CPT by activating ATM and DNA-PKcs pathways. We find that, once activated, these sensor kinases propagate signals to downstream effectors that lead to H2AX and p53 phosphorylation and culminate in high apoptotic rate. Moreover, we determined that the apoptotic process encompasses PS exposure, caspase-9 and caspase-3 activation, PARP cleavage and DNA fragmentation. Remarkably, the high apoptosis displayed by hESCs seems not to be only a specific response to CPT, as elevated apoptosis rates have been observed after exposure to UV, ionizing radiation, and other DNA-damaging agents (Hyka-Nouspikel et al., 2012). It thus appears that the high propensity to apoptosis is a common characteristic of hESCs, perhaps a strategy to ensure genomic integrity by favoring apoptosis over DNA repair.

Importantly, in this study we also determined that the use of small molecule inhibitors that impair ATM or DNA-PKcs activity further sensitizes hESCs to CPT treatment. In this sense, recruitment of kinase-dead ATM to sites of DNA damage was found to occur normally (Daniel et al., 2012). Furthermore, autophosphorylation of DNA-PK is thought to be necessary for events after recruitment of DNA-PKcs to DSBs and for its ultimate dissociation (Reddy et al., 2004). Thus, catalytically inhibited ATM or DNA-PK may impair the function of repair factors by occluding their access to DSBs and severely disturb the ability of cells to respond to damage.

Conflicting evidence has been reported as to whether p53 is functional or non-functional in ES cells. However, despite the nonfunctional p53-dependent G1/S checkpoint pathway, p53 protein has been shown to be stabilized and activated in hESCs in response to gamma or UVC irradiation and to etoposide (Grandela et al., 2007; Hyka-Nouspikel et al., 2012). Herein, we present evidence that CPT treatment leads to p53 stabilization and nuclear localization, supporting the concept that this tumor suppressor is functional in hESCs. Moreover, in the molecular setting displayed by hESCs, the proapoptotic activity of p53 might prevail. Recently, it has been reported that healthy undifferentiated H9 cells maintain Bax in its preactivated state at the Golgi, in contrast to what occur in other cell types in which Bax is typically present in an inactive form in the cytosol (Dumitru et al., 2012). Interestingly, in the same manuscript researchers found that upon etoposide exposure, active Bax translocates from the Golgi to the mitochondria in a p53-dependent manner. In this sense, the CPT-induced programmed cell death achieved in the presence of an operative p53′ mitochondrial program supports this concept.

At this point it is important to mention that although apoptotic signals are generally mediated through two caspase-dependent molecular pathways, namely, intrinsic and extrinsic cascades, a third molecular pathway of programmed cell death does exist. This pathway is characterized by nuclear

translocation of apoptosis-inducing factor and endonuclease G (EndoG) that trigger chromatin condensation and DNA fragmentation independent of caspase activation (Galluzzi et al., 2008). To this end, Tichy et al. (2013) recently reported that, after etoposide treatment, mouse ESCs undergo charontosis, a novel programmed cell death pathway, dependent upon p53 and EndoG. Importantly, in the mentioned study, researchers find that PFT-μ addition reduces this novel type of cell death. Thus, we cannot discard the possibility that charontosis is also operative in hESCs.

Although p53 is stabilized and phosphorylated upon CPT exposure, no $p21^{Waf1}$ protein was detectable in damaged undifferentiated H9 cells. In somatic cells, $p21^{Waf1}$ appears to be a principal mediator of cell cycle arrest in response to different types of DNA damage, not only by inactivating G1-phase cyclins/CDKs complexes, but also through other processes, which possibly include direct interaction with PCNA to inhibit DNA replication, and indirect effects mediated by interaction with other cell cycle regulators (Cazzalini et al., 2010). To this end, Mauro et al. have recently reported that $p21^{Waf1}$ plays a central role in the coordination of early steps of DNA replication coupled to DSB repair triggered by the DSB-inducing agents mitomycin C, CPT and etoposide (Mauro et al., 2012). Importantly, in their study they determined that human and murine $p21^{Waf1}$ deficient cells are hypersensitive to the mentioned genotoxics.

On the other hand, an active role for $p21^{Waf1}$ in inhibiting apoptosis has been described in several contexts. Indeed, $p21^{Waf1}$ was reported to have an antiapoptotic activity through the inhibition of CDK activity required for activation of the caspase cascade downstream of mitochondria (Cazzalini et al., 2010; Janicke et al., 2007). Thus the absence of $p21^{Waf1}$ to ensure DNA repair and reduce apoptosis may be another hallmark of hESCs to rapidly undergo apoptosis in early stages of development upon encountering DNA damage.

The integration of opposing signals (e.g. repair DNA or apoptosis) into a cellular consensus decision may require significantly more complexity in somatic cells than in ES cells, where a very limited number of signaling pathways suffice for control of proliferation and survival. As differentiation proceeds the cell cycle structure and apoptotic machinery undergo dynamic changes. For instance, hESCs exhibit high levels of CDK activity which is a consequence of the absence or very weak expression of CKIs (Koledova et al., 2010). As described herein hESC differentiation occurred concomitantly with changes in cell cycle structure and robust induction of CKIs, particularly $p21^{Waf1}$ (Fig. 4). These changes may account for the increase in cell viability exhibited by CPT-treated EBs. Consistently, in this sense, Dumitru et al. reported that while undifferentiated H9 hESCs have constitutively active Bax and undergo rapid apoptosis in response to DNA damage, differentiated counterparts have no constitutively active Bax, and are no longer highly sensitive to DNA damage (Dumitru et al., 2012). As a whole, these results open new questions: are the atypical cell cycle structure, the absence of $p21^{Waf1}$, the presence of activated Bax and other, as yet, undetermined features, hallmarks of hESC that endow them with the ability to rapidly undergo apoptosis and thus maintain a pristine population of pluripotent cells?

The genetic stability of hESCs has acquired a special significance as research moves toward developing applications in regenerative medicine for the differentiated derivatives of these cells. Thus, all attempts to define the mechanisms mounted by hESC to cope with genomic threats could shed light on the knowledge of stem cell biology and further use in medicine.

Supplementary data to this article can be found online at http://dx.doi.org/10.1016/j.scr.2013.12.002.

Acknowledgments

This work was supported by research grants from Consejo Nacional de Investigaciones Científicas y Técnicas (CONICET) and Agencia Nacional de Promoción Científica y Tecnológica (ANPCYT). CPG is a Graduate Fellow and SGM is a Research Member of CONICET. GAVR is a Graduate Fellow of Instituto Nacional del Cáncer. LR is a Posdoctoral Fellow of Fundación Bunge y Born. The authors would like to thank Damian D. Fernandez Espinosa for his skillful technical assistance.

References

Abraham, R.T., 2004. PI 3-kinase related kinases: 'big' players in stress-induced signaling pathways. DNA Repair (Amst) 3 (8–9), 883–887. http://dx.doi.org/10.1016/j.dnarep.2004.04.002.

Adams, B.R., Golding, S.E., Rao, R.R., Valerie, K., 2010. Dynamic dependence on ATR and ATM for double-strand break repair in human embryonic stem cells and neural descendants. PLoS One 5 (4), e10001. http://dx.doi.org/10.1371/journal.pone.0010001.

An, J., Huang, Y.C., Xu, Q.Z., Zhou, L.J., Shang, Z.F., Huang, B., Zhou, P.K., 2010. DNA-PKcs plays a dominant role in the regulation of H2AX phosphorylation in response to DNA damage and cell cycle progression. BMC Mol. Biol. 11, 18. http://dx.doi.org/10.1186/1471-2199-11-18.

Ang, B.T., Yap, E., Lim, J., Tan, W.L., Ng, P.Y., Ng, I., Yeo, T.T., 2003. Poly(adenosine diphosphate-ribose) polymerase expression in human traumatic brain injury. J. Neurosurg. 99 (1), 125–130. http://dx.doi.org/10.3171/jns.2003.99.1.0125.

Arnaudeau, C., Lundin, C., Helleday, T., 2001. DNA double-strand breaks associated with replication forks are predominantly repaired by homologous recombination involving an exchange mechanism in mammalian cells. J. Mol. Biol. 307 (5), 1235–1245. http://dx.doi.org/10.1006/jmbi.2001.4564.

Barta, T., Vinarsky, V., Holubcova, Z., Dolezalova, D., Verner, J., Pospisilova, S., Hampl, A., 2010. Human embryonic stem cells are capable of executing G1/S checkpoint activation. Stem Cells 28 (7), 1143–1152. http://dx.doi.org/10.1002/stem.451.

Becker, K.A., Ghule, P.N., Therrien, J.A., Lian, J.B., Stein, J.L., van Wijnen, A.J., Stein, G.S., 2006. Self-renewal of human embryonic stem cells is supported by a shortened G1 cell cycle phase. J. Cell. Physiol. 209 (3), 883–893. http://dx.doi.org/10.1002/jcp.20776.

Borriello, A., Caldarelli, I., Bencivenga, D., Criscuolo, M., Cucciolla, V., Tramontano, A., Della Ragione, F., 2011. p57(Kip2) and cancer: time for a critical appraisal. Mol. Cancer Res. 9 (10), 1269–1284. http://dx.doi.org/10.1158/1541-7786.MCR-11-0220.

Callen, E., Jankovic, M., Wong, N., Zha, S., Chen, H.T., Difilippantonio, S., Nussenzweig, M., 2009. Essential role for DNA-PKcs in DNA double-strand break repair and apoptosis in ATM-deficient lymphocytes. Mol. Cell 34 (3), 285–297. http://dx.doi.org/10.1016/j.molcel.2009.04.025.

Cazzalini, O., Scovassi, A.I., Savio, M., Stivala, L.A., Prosperi, E., 2010. Multiple roles of the cell cycle inhibitor p21(CDKN1A) in the DNA damage response. Mutat. Res. 704 (1–3), 12–20. http://dx.doi.org/10.1016/j.mrrev.2010.01.009.

Chen, B.P., Chan, D.W., Kobayashi, J., Burma, S., Asaithamby, A., Morotomi-Yano, K., Chen, D.J., 2005. Cell cycle dependence of

DNA-dependent protein kinase phosphorylation in response to DNA double strand breaks. J. Biol. Chem. 280 (15), 14709–14715 (doi: M408827200).

Chipuk, J.E., Kuwana, T., Bouchier-Hayes, L., Droin, N.M., Newmeyer, D.D., Schuler, M., Green, D.R., 2004. Direct activation of Bax by p53 mediates mitochondrial membrane permeabilization and apoptosis. Science 303 (5660), 1010–1014. http://dx.doi.org/10.1126/science.1092734.

Daniel, J.A., Pellegrini, M., Lee, B.S., Guo, Z., Filsuf, D., Belkina, N.V., Nussenzweig, A., 2012. Loss of ATM kinase activity leads to embryonic lethality in mice. J. Cell Biol. 198 (3), 295–304. http://dx.doi.org/10.1083/jcb.201204035.

Dumitru, R., Gama, V., Fagan, B.M., Bower, J.J., Swahari, V., Pevny, L.H., Deshmukh, M., 2012. Human embryonic stem cells have constitutively active Bax at the Golgi and are primed to undergo rapid apoptosis. Mol. Cell 46 (5), 573–583. http://dx.doi.org/10.1016/j.molcel.2012.04.002.

Filion, T.M., Qiao, M., Ghule, P.N., Mandeville, M., van Wijnen, A.J., Stein, J.L., Stein, G.S., 2009. Survival responses of human embryonic stem cells to DNA damage. J. Cell. Physiol. 220 (3), 586–592. http://dx.doi.org/10.1002/jcp.21735.

Filipczyk, A.A., Laslett, A.L., Mummery, C., Pera, M.F., 2007. Differentiation is coupled to changes in the cell cycle regulatory apparatus of human embryonic stem cells. Stem Cell Res. 1 (1), 45–60. http://dx.doi.org/10.1016/j.scr.2007.09.002.

Galluzzi, L., Joza, N., Tasdemir, E., Maiuri, M.C., Hengartner, M., Abrams, J.M., Kroemer, G., 2008. No death without life: vital functions of apoptotic effectors. Cell Death Differ. 15 (7), 1113–1123. http://dx.doi.org/10.1038/cdd.2008.28.

Gonzalez, T., Seoane, M., Caamano, P., Vinuela, J., Dominguez, F., Zalvide, J., 2003. Inhibition of Cdk4 activity enhances translation of p27kip1 in quiescent Rb-negative cells. J. Biol. Chem. 278 (15), 12688–12695. http://dx.doi.org/10.1074/jbc.M207530200.

Grandela, C., Pera, M.F., Grimmond, S.M., Kolle, G., Wolvetang, E.J., 2007. p53 is required for etoposide-induced apoptosis of human embryonic stem cells. Stem Cell Res. 1 (2), 116–128. http://dx.doi.org/10.1016/j.scr.2007.10.003.

Hyka-Nouspikel, N., Desmarais, J., Gokhale, P.J., Jones, M., Meuth, M., Andrews, P.W., Nouspikel, T., 2012. Deficient DNA damage response and cell cycle checkpoints lead to accumulation of point mutations in human embryonic stem cells. Stem Cells 30 (9), 1901–1910. http://dx.doi.org/10.1002/stem.1177.

Janicke, R.U., Sohn, D., Essmann, F., Schulze-Osthoff, K., 2007. The multiple battles fought by anti-apoptotic p21. Cell Cycle 6 (4), 407–413 (doi: 3855).

Kapinas, K., Grandy, R., Ghule, P., Medina, R., Becker, K., Pardee, A., Stein, G., 2013. The abbreviated pluripotent cell cycle. J. Cell. Physiol. 228 (1), 9–20. http://dx.doi.org/10.1002/jcp.24104.

Kobayashi, J., Tauchi, H., Chen, B., Burma, S., Tashiro, S., Matsuura, S., Komatsu, K., 2009. Histone H2AX participates the DNA damage-induced ATM activation through interaction with NBS1. Biochem. Biophys. Res. Commun. 380 (4), 752–757. http://dx.doi.org/10.1016/j.bbrc.2009.01.109.

Koledova, Z., Kramer, A., Kafkova, L.R., Divoky, V., 2010. Cell-cycle regulation in embryonic stem cells: centrosomal decisions on self-renewal. Stem Cells Dev. 19 (11), 1663–1678. http://dx.doi.org/10.1089/scd.2010.0136.

Liu, L.F., Desai, S.D., Li, T.K., Mao, Y., Sun, M., Sim, S.P., 2000. Mechanism of action of camptothecin. Ann. N. Y. Acad. Sci. 922, 1–10.

Lu, X., 2005. p53: a heavily dictated dictator of life and death. Curr. Opin. Genet. Dev. 15 (1), 27–33 (doi: S0959-437X(04)00194-7).

Martin, M., Terradas, M., Tusell, L., Genesca, A., 2012. ATM and DNA-PKcs make a complementary couple in DNA double strand break repair. Mutat. Res. 751 (1), 29–35 (doi: S1383-5742(11)00119-0).

Mauro, M., Rego, M.A., Boisvert, R.A., Esashi, F., Cavallo, F., Jasin, M., Howlett, N.G., 2012. p21 promotes error-free replication-coupled DNA double-strand break repair. Nucleic Acids Res. 40 (17), 8348–8360 (doi: gks612).

Momcilovic, O., Choi, S., Varum, S., Bakkenist, C., Schatten, G., Navara, C., 2009. Ionizing radiation induces ataxia telangiectasia mutated-dependent checkpoint signaling and G(2) but not G(1) cell cycle arrest in pluripotent human embryonic stem cells. Stem Cells 27 (8), 1822–1835. http://dx.doi.org/10.1002/stem.123.

Oren, M., 2003. Decision making by p53: life, death and cancer. Cell Death Differ. 10 (4), 431–442. http://dx.doi.org/10.1038/sj.cdd.4401183.

Pera, M.F., Reubinoff, B., Trounson, A., 2000. Human embryonic stem cells. J. Cell Sci. 113 (Pt 1), 5–10.

Pommier, Y., 2006. Topoisomerase I inhibitors: camptothecins and beyond. Nat. Rev. Cancer 6 (10), 789–802 (doi: nrc1977).

Pommier, Y., Cherfils, J., 2005. Interfacial inhibition of macromolecular interactions: nature's paradigm for drug discovery. Trends Pharmacol. Sci. 26 (3), 138–145 (doi: S0165-6147(05)00027-1).

Rao, V.A., Fan, A.M., Meng, L., Doe, C.F., North, P.S., Hickson, I.D., Pommier, Y., 2005. Phosphorylation of BLM, dissociation from topoisomerase IIIalpha, and colocalization with gamma-H2AX after topoisomerase I-induced replication damage. Mol. Cell. Biol. 25 (20), 8925–8937 (doi: 25/20/8925).

Reddy, Y.V., Ding, Q., Lees-Miller, S.P., Meek, K., Ramsden, D.A., 2004. Non-homologous end joining requires that the DNA-PK complex undergo an autophosphorylation-dependent rearrangement at DNA ends. J. Biol. Chem. 279 (38), 39408–39413. http://dx.doi.org/10.1074/jbc.M406432200.

Romorini, L., Scassa, M.E., Richardson, G.V., Bluguermann, C., de Giusti, C.J., Questa, M., Miriuka, S.G., 2012. Activation of apoptotic signalling events in human embryonic stem cells upon Coxsackievirus B3 infection. Apoptosis 17 (2), 132–142. http://dx.doi.org/10.1007/s10495-011-0668-z.

Rotman, G., Shiloh, Y., 1999. ATM: a mediator of multiple responses to genotoxic stress. Oncogene 18 (45), 6135–6144. http://dx.doi.org/10.1038/sj.onc.1203124.

Scassa, M.E., Jaquenod de Giusti, C., Questa, M., Pretre, G., Richardson, G.A., Bluguermann, C., Gomez, R.M., 2011. Human embryonic stem cells and derived contractile embryoid bodies are susceptible to Coxsakievirus B infection and respond to interferon Ibeta treatment. Stem Cell Res. 6 (1), 13–22. http://dx.doi.org/10.1016/j.scr.2010.09.002.

Sedelnikova, O.A., Pilch, D.R., Redon, C., Bonner, W.M., 2003. Histone H2AX in DNA damage and repair. Cancer Biol. Ther. 2 (3), 233–235 (doi: 373).

Sordet, O., Redon, C.E., Guirouilh-Barbat, J., Smith, S., Solier, S., Douarre, C., Pommier, Y., 2009. Ataxia telangiectasia mutated activation by transcription- and topoisomerase I-induced DNA double-strand breaks. EMBO Rep. 10 (8), 887–893. http://dx.doi.org/10.1038/embor.2009.97.

Strom, E., Sathe, S., Komarov, P.G., Chernova, O.B., Pavlovska, I., Shyshynova, I., Gudkov, A.V., 2006. Small-molecule inhibitor of p53 binding to mitochondria protects mice from gamma radiation. Nat. Chem. Biol. 2 (9), 474–479 (doi: nchembio809).

Strumberg, D., Pilon, A.A., Smith, M., Hickey, R., Malkas, L., Pommier, Y., 2000. Conversion of topoisomerase I cleavage complexes on the leading strand of ribosomal DNA into 5′-phosphorylated DNA double-strand breaks by replication runoff. Mol. Cell. Biol. 20 (11), 3977–3987.

Thomson, J.A., Itskovitz-Eldor, J., Shapiro, S.S., Waknitz, M.A., Swiergiel, J.J., Marshall, V.S., Jones, J.M., 1998. Embryonic stem cell lines derived from human blastocysts. Science 282 (5391), 1145–1147.

Tian, X.J., Liu, F., Zhang, X.P., Li, J., Wang, W., 2012. A two-step mechanism for cell fate decision by coordination of nuclear and mitochondrial p53 activities. PLoS One 7 (6), e38164. http://dx.doi.org/10.1371/journal.pone.0038164.

Tichy, E.D., Stephan, Z.A., Osterburg, A., Noel, G., Stambrook, P.J., 2013. Mouse embryonic stem cells undergo charontosis, a novel programmed cell death pathway dependent upon cathepsins, p53, and EndoG, in response to etoposide treatment. Stem Cell Res. 10 (3), 428–441. http://dx.doi.org/10.1016/j.scr.2013.01.010.

Vaseva, A.V., Moll, U.M., 2009. The mitochondrial p53 pathway. Biochim. Biophys. Acta 1787 (5), 414–420. http://dx.doi.org/10.1016/j.bbabio.2008.10.005.

Wang, Y., Blelloch, R., 2009. Cell cycle regulation by microRNAs in embryonic stem cells. Cancer Res. 69 (10), 4093–4096. http://dx.doi.org/10.1158/0008-5472.CAN-09-0309.

Ward, I.M., Chen, J., 2001. Histone H2AX is phosphorylated in an ATR-dependent manner in response to replicational stress. J. Biol. Chem. 276 (51), 47759–47762. http://dx.doi.org/10.1074/jbc.C100569200.

Yu, F., Megyesi, J., Safirstein, R.L., Price, P.M., 2005. Identification of the functional domain of p21(WAF1/CIP1) that protects cells from cisplatin cytotoxicity. Am. J. Physiol. Renal Physiol. 289 (3), F514–F520 (doi: 00101.2005).

Zaika, E., Wei, J., Yin, D., Andl, C., Moll, U., El-Rifai, W., Zaika, A.I., 2011. p73 protein regulates DNA damage repair. FASEB J. 25 (12), 4406–4414. http://dx.doi.org/10.1096/fj.11-192815.

Zhang, X.P., Liu, F., Wang, W., 2010. Coordination between cell cycle progression and cell fate decision by the p53 and E2F1 pathways in response to DNA damage. J. Biol. Chem. 285 (41), 31571–31580. http://dx.doi.org/10.1074/jbc.M110.134650.

Zhao, H., Traganos, F., Darzynkiewicz, Z., 2008. Phosphorylation of p53 on Ser15 during cell cycle caused by Topo I and Topo II inhibitors in relation to ATM and Chk2 activation. Cell Cycle 7 (19), 3048–3055 (doi: 6750).